Cross-diffusion Waves in Hydro-Poro-Mechanics

Manman Hu[a,b,*], Christoph Schrank[c], Klaus Regenauer-Lieb[b]

[a] *Department of Civil Engineering, The University of Hong Kong, Pokfulam, Hong Kong, China*

[b] *School of Minerals and Energy Resources Engineering, The University of New South Wales, Sydney, NSW 2033 Australia*

[c] *Science and Engineering Faculty, Queensland University of Technology, Brisbane, QLD, 4001, Australia*

Abstract

We propose a new class of wave-phenomena in multiphase solids (and granular media) triggered by Hydro-Poro-Mechanical coupling and cross-diffusion feedbacks of porous materials. We define cross-diffusion as the phenomenon when a generalized thermodynamic force induces a generalized thermodynamic flux of another kind. Addition of cross-diffusion relaxes the adiabatic constraints on the reaction part of the system and corrects the mathematical ill-posedness. We identify the important aspect of cross-diffusion terms and present a linear stability analysis of the governing partial differential equations (PDE's). Multiple transient wave instabilities are found as solutions of the coupled PDE's. In the long-wavelength limit (long-time scale) these waves feed into solitary waves that are standing wave patterns frozen into the porous medium at various scales. We revisit earlier work showing that the wavenumber of the standing wave is entirely defined by the ratio of the mechanical over the fluid (self-diffusion) coefficients of the coupled reaction-cross-diffusion equations. Diffusion coefficients are hence identified as material parameters controlling the criterion for nucleation of waves and the signature of both transient cross- and stationary self-diffusion waves. We show examples of self- and cross-diffusion waves in nature and laboratory experiments as stationary and time-lapse diffusional waves. Our approach offers a simple mathematical framework for analysis of coupled hydro-mechanical porous medium, providing a new fundamental perspective for analyses of

*Corresponding author

Email address: mmhu@hku.hk (Manman Hu)

the initiation of macroscopic instabilities and transient precursors in many disciplines.

Keywords: reaction-diffusion systems, coupled processes, solid-fluid interaction, pattern formation, porous media, hydro-mechanics

1. Introduction

We present a simple approach for the interpretation and analysis of spatio-temporal patterns triggered by coupled hydro-mechanical reaction-diffusion feedback process in porous systems that are post-yield. We formulate the problem in a generalized far from equilibrium thermodynamic framework, where we consider coupling of two hydro-mechanical reaction-diffusion equations. Patterns observed in analogous chemical far from equilibrium reaction-diffusion systems are generally interpreted as dissipative or non-equilibrium Turing patterns, standing waves, propagating wave instabilities and other dissipative matter or energy phenomena (Vanag and Epstein, 2009).

We investigate in this paper whether the importance of cross-diffusion processes discovered in chemistry (Vanag and Epstein, 2009) also applies to the mathematically equivalent Hydro-Poro-Mechanical reaction-diffusion systems. Cross-diffusional waves have only recently been classified as a new class of excitation waves (Tsyganov et al., 2007; Biktashev and Tsyganov, 2016). We propose that in porous media cross-diffusional waves can readily be encountered in nature and the laboratory. They offer a simple and elegant way forward for interpretation and analysis of hydro-mechanical coupled phenomena in poro-mechanics of multiphase matter and granular media flow. In the following we identify the important aspect of cross-diffusion terms in a generalized Hydro-Poro-Mechanical reaction-diffusion systems and summarise a linear stability analysis of the governing partial differential equations. These cross-diffusion terms become active after initial yield. We show here that they play an important role in the processes leading to macroscopic localization of plastic deformation.

Post-yield the macroscopic criterion for localization is already well-known to be an acceleration wave phenomenon (Rudnicki and Rice, 1975; Rice, 1976). By using a post-yield overstress approach (Perzyna, 1966) we follow the conceptual time-independent generalization of the acceleration wave approach from shear localization (Rudnicki and Rice, 1975; Rice, 1976) to volumetric internal processes in porous solids as proposed by Veveakis and

Regenauer-Lieb (2015) and extend it to the transient time-dependent wave propagation phenomenon in porous media.

In continuum mechanics, compatibility of the deformation gradient is considered as a necessary and sufficient condition for an allowable single-valued continuous field in a simply-connected body. Based on the Beltrami-Michell compatibility condition and stress equilibrium condition, Rice and Cleary (1976) arrived at a total stress diffusion equation for compressing a fully saturated poroelastic material. Here, we decompose the total stress into a fluid pressure and a Perzyna visco-plastic overstress of the solid skeleton and use mixture theory to combine the two. We also ignore any elastic deformation and assume elastic incompressibility of fluids and solids. In order to propose a mathematically simple approach for localization phenomena triggered by pressure waves, we simplify the Perzyna overstress approach into a scalar 1-D representation of volumetric processes. This approach is consistent with practical applications of consolidation theory, where incorporating three-dimensional flow vectors is complicated and only applicable to a very limited range of problems. In this sense we follow the geo-technical engineering practice, where for the vast majority of consolidation problems, the assumption that fluid flow and mechanical strains take place in one direction only, is sufficient (Atkinson, 2014).

In this sense we identify the 1-D framework as the post-yield diffusional overstress in a formal analogy between plastic solids and viscous fluids developed originally for rigid-plastic bodies by Hill (1954). The approach identifies the stress tensor by the properties of a fluid field (i.e. pressure, density and velocity) satisfying conservation equations of continuity and motion. Hence, no additional compatibility condition is required. Hill (1954) notes that by application of a proper yield criterion the distribution of stress in an ideal plastic body corresponds to the counterpart of a fluid field, based on the assumption of homo-entropic flow. Homo-entropic flow means that the entropy is homogeneous in the considered continuum volume and there is no heat transfer. The pressure is hence dependent on the density function only. This simplification is not a necessary condition for the presented approach as it can be easily extended to include other diffusional gradients by consideration of the thermal reaction-diffusion equation. However, for clarity we adopt in what follows Hill's hydrodynamic analogy for a fully rigid-plastic solid in a strict sense and use the conservation of continuity as a dynamic compatibility condition, which is encompassed in mixture theory.

The paper is organized as follows. With a brief review of overstress formu-

lation, we first formulate time-dependent conservation laws for consolidation processes based on thermodynamic considerations. Then we follow the classical mixture theory approach for identifying the role of cross-diffusion as a microstructural element stemming from internal mass-transfer in the thermodynamic conservation laws. We subsequently introduce the momentum balance and derive a cnoidal wave solution as the nonlinear-periodic solution of the Korteweg-de-Vries equation. Cnoidal waves appear as a volumetric material instability if a non-linear constitutive equation (power law) is used for the solid matrix. We show that in the long-wavelength limit these waves appear as solitary standing waves equivalent to the classical shear localization instability criterion in plasticity where the wave speed of acceleration waves is set to zero (Rudnicki and Rice, 1975; Rice, 1976). In order to derive the transient solution we first consider the classical case of two consolidation processes where the time scales of consolidation are far apart allowing the two steady state solutions to be independent of each other.

Subsequently, we focus on the cross-over regime between the primary and the secondary consolidation, where additional transient cross-diffusional wave instabilities might arise due to the tight coupling between micro-processes in at least two phases. These waves are of shorter wavelength than the standing cnoidal waves and we argue that they may play an important role in the transient processes leading to the formation of the long-wavelength material instability. Based on mixture theory, we further consider the process of inter-constituent mass transfer, which corresponds to the cross-diffusion terms in the proposed conservation laws. The onset of the Hydro-Poro-Mechanical wave instability is derived via a linear stability analysis of the governing equations. A field example of creeping cross-diffusion waves in a partially molten rock, laboratory examples of grain-crushing induced cross-diffusion waves in a granular medium and a porous rock are presented as a closure of this paper.

2. Overstress formulation

In this paper we decompose the mechanical behaviour of a solid before and after yield into linear elasticity and visco-plastic flow, respectively. This approach considers that only after entering the plastic state, the material starts to manifest its viscous flow properties. The strain rate $\dot{\epsilon}_{ij}$ is hence decomposed into an elastic and an inelastic part:

$$\dot{\epsilon}_{ij} = \dot{\epsilon}^{e}_{ij} + \dot{\epsilon}^{vp}_{ij}, \tag{1}$$

where the elastic part $\dot{\epsilon}^{e}_{ij}$ denotes the strain rate inherited from the elastic region of the material, where no viscous properties are considered. $\dot{\epsilon}^{vp}_{ij}$ denotes the visco-plastic component of the strain rate, and is assumed to follow an associative flow law:

$$\dot{\epsilon}^{vp}_{ij} = \dot{\lambda}\frac{f}{\sigma'_{ij}}, \tag{2}$$

where f denotes the yield function, $\dot{\lambda}$ a non-negative scalar multiplier, representing the magnitude of the visco-plastic strain rate. σ'_{ij} denotes the effective stress, which is expressed as

$$\sigma'_{ij} = \sigma_{ij} - bp_f\delta_{ij}, \tag{3}$$

where σ_{ij} denotes the total stress tensor, p_f the fluid pressure, b Biot's coefficient and δ_{ij} Kronecker's delta. In the context of visco-plastic matrix, the Biot's coefficient can be conveniently assumed as 1.

Using Perzyna (1966)'s overstress model for visco-plasticity, we have an explicit expression for the plastic multiplier:

$$\dot{\lambda} = \frac{\langle\bar{\varphi}(f)\rangle}{\eta_s}, \tag{4}$$

where η_s denotes the viscosity of the visco-plastic solid matrix, $\bar{\varphi}$ the overstress function dependent on the yield surface f. The symbol $\langle\cdot\rangle$ denotes the Macaulay brackets, and is defined as follows:

$$\langle\bar{\varphi}(f)\rangle = \begin{cases} \bar{\varphi}(f), & \text{if } \bar{\varphi}(f) \geq 0; \\ 0, & \text{otherwise.} \end{cases} \tag{5}$$

With a Taylor expansion of the overstress function around the effective yield limit σ'_Y, the incremental visco-plastic strain is related to the increment of the overstress $\bar{\sigma}_{ij} = \sigma'_{ij} - \sigma'_Y$ in power series.

3. Thermodynamic considerations: 1-D consolidation

Since we are interested in formulating a dynamic process we need to ensure consistency with thermodynamic principles. For this we formulate the time derivative conservation laws in terms of balance laws of thermodynamic fluxes and thermodynamic forces with source terms. Thermodynamic pairs

of conjugate variables (i.e. generalized forces and fluxes) in a Hydro-Poro-Mechanical coupled system are defined in Table 1. The conservation laws are derived based on the thermodynamic principle that a generalized flux is induced by the gradient of a generalized force. D_H and D_M are diffusional coefficients that correspond to the effective bulk modulus of the primary and the secondary consolidation (Coussy, 2004), respectively. The framework in Table 1 can readily be extended to three-dimensional representations; however in this paper we focus on the cross-scale analysis of dynamic consolidation processes and elaborate in particular on how the cross-diffusional waves are initiated under 1-D assumption.

The primary consolidation process, in the sense of classical poromechanics, features the diffusion of pore fluid pressure (e.g. melt in partially molten rock) and this process (H) can be described by Darcy's law, which makes the diffusion coefficient D_H dependent on the matrix permeability and melt viscosity. The secondary consolidation is the compaction of the viscous solid matrix after yielding and the mechanical flux (M) represents the 1-D incremental change in solid-phase visco-plastic overstress $\bar{p}_s = \langle p' - p_Y \rangle$ where p' denotes the volumetric mean effective stress $p' = p - p_f$ and p_Y the volumetric yield stress. $\langle \cdot \rangle$ denotes the Macaulay brackets. p and p_f are the total pressure and fluid pressure, respectively. The capital $D(\cdot)/Dt$ denotes the material derivative.

Table 1: Generalized Thermodynamic Fluxes and Forces in a Hydro-Poro-Mechanical coupled system (1-D). Basic conservation laws (without cross-diffusion) are derived based on the thermodynamic principle that a thermodynamic flux is driven by the gradient of a thermodynamic force.

1-D Hydro-Poro-Mechanics based on thermodynamics			
	Thermodynamic Force (1-D)	Thermodynamic Flux (1-D)	Conservation Law (no cross-diffusion)
H	$F_H = \frac{\partial p_f}{\partial x}$	$q_H = -\frac{Dp_f}{Dt}$	$\frac{Dp_f}{Dt} = D_H \frac{\partial F_H}{\partial x} + r^f$
M	$F_M = \frac{\partial \bar{p}_s}{\partial x}$	$q_M = -\frac{D\bar{p}_s}{Dt}$	$\frac{D\bar{p}_s}{Dt} = D_M \frac{\partial F_M}{\partial x} + r^M$

For consolidation of the solid skeleton we refer to the work of Hill (1962) who identified the role of acceleration waves with a wave speed that is dependent on the properties governing the deformation rate and distinguished

from the elastic wave phenomenon. Rice (1976) identified the localisation phenomenon as an acceleration wave with vanishing wave speed. The mode of localisation is dependent on the polarization vector of the acceleration wave of vanishing speed. In the rigid-plastic analogy the localisation problem can hence be stated as a solution on the characteristics of the hyperbolic PDE's. We follow the extension from acceleration waves in shear deformation to the acceleration waves in volumetric deformation (Veveakis and Regenauer-Lieb, 2015) to arrive at the conservation law for dissipative pressure waves.

Accordingly, the mechanical (M) conservation law in the creeping flow regime is described as a diffusion wave equation (no inertia) travelling at a wave velocity $v = Dx/Dt$ (turning $\frac{D\bar{p}_s}{Dt}$ into $v\frac{D\bar{p}_s}{Dx}$ in Table 1). r^f and r^M denote possible reactive source terms. In classical poromechanics, the two diffusional time-scales of the consolidation processes are considered to be sufficiently far apart. However, under many circumstances that involve viscous deformation, such as a partially molten rock under geodynamic loading, this is not likely to be the case.

In order to consider possible time dependent interactions between the solid and fluid thermodynamic forces and fluxes at micro-structural scale, we refer to the concept of cross-diffusion which in a complex system is defined by the phenomenon that a gradient of one generalized thermodynamic force can drive another generalized thermodynamic flux. Now, the off-diagonal elements in the augmented diffusion matrix can be non-zero. Assuming linear superposition of cross-diffusion terms, we rewrite the conservation laws in 1-D as:

$$\frac{Dp_f}{Dt} = D_H \frac{\partial^2 p_f}{\partial x^2} + h_1 \frac{\partial^2 \bar{p}_s}{\partial x^2} + r^f \tag{6a}$$

$$\frac{D\bar{p}_s}{Dt} = D_M \frac{\partial^2 \bar{p}_s}{\partial x^2} + h_2 \frac{\partial^2 p_f}{\partial x^2} + r^M. \tag{6b}$$

where h_1 and h_2 are the cross-diffusion coefficients (Vanag and Epstein, 2009), which for sufficiently large values can trigger wave instabilities from e.g. time-dependent internal mass transfer. We will discuss in Section 6 the results of a linear stability analysis (Eq. 29). This shows that for a system described by Eq. 6 the addition of the cross-diffusional terms can give rise to a new style of instabilities if h_1 and h_2 are of opposite sign and their conjoint negative contribution to the perturbation is stronger than the classical diffusion of mechanical and fluid pressures via poroviscoplastic

relaxation of matrix stress and Darcy's law, respectively.

An opposite sign of the two cross-diffusion coefficients is required for an instability. A discussion on thermodynamic consistency and comments on the Onsager Theorem of the cross-diffusion matrix can be found in (Biktashev and Tsyganov, 2016). The cross-diffusion terms in Eq. 6 can be derived from mixture theory by considering the process of inter-constituent mass transfer at pore-scale and relaxing the adiabatic constraints on the reaction part of the system (see Section 4). In the field example (see Fig. 5) we identify at least three diffusional length scales: h, l_1 and l_2, corresponding to the large-scale Hydro-Poro-Mechanical instability forming the compaction band and two cross-diffusional length scales adjacent to the band itself, respectively. These length-scales define the wavenumbers of the coupled Hydro-Poro-Mechanical transient cross-diffusional waves.

4. Mass balance of a two-constituent mixture

We consider a representative elementary volume (REV) of a two-constituent mixture, e.g. a fully saturated porous medium, as shown in Fig. 1. The volume fraction of the pore space (i.e. the fluid phase) is defined as the bulk porosity:

$$\phi = \frac{V_f}{V_{REV}} = 1 - \frac{V_s}{V_{REV}}, \tag{7}$$

where V_{REV}, V_f and V_s denote the REV volume, the volume of the fluid phase and that of the solid phase in the REV, respectively.

Mass conservation for the fluid phase and the solid phase in 1-D gives

$$\frac{\partial[\rho_f V_f]}{\partial t} + \frac{\partial[\rho_f V_f v_f]}{\partial x} = \dot{\xi}_f V_{REV}, \tag{8a}$$

$$\frac{\partial[\rho_s V_s]}{\partial t} + \frac{\partial[\rho_s V_s v_s]}{\partial x} = \dot{\xi}_s V_{REV}, \tag{8b}$$

respectively. ρ_f and ρ_s denote the density of the solid skeleton and the fluid density, while v_f and v_s are defined as the fluid and solid flow velocities (in the direction of x). $\dot{\xi}_f$ represents the mass generation rate in the fluid phase (e.g. mineral mass diffusing into fluid from the solid skeleton, internal erosion of the solid into fluid) per unit volume inside the REV, and $\dot{\xi}_s$ the mass generation rate (i.e. the opposite of the mass removal rate) in the solid phase per unit volume in the REV.

Substituting Eq. 7 into Eq. 17 and eliminating V_{REV}, we have

$$\frac{\partial[\rho_f \phi]}{\partial t} + \underbrace{\frac{\partial[\rho_f \phi v_f]}{\partial x}}_{Self-diffusion} = \dot{\xi}_f^{REV}, \tag{9a}$$

$$\frac{\partial[\rho_s (1-\phi)]}{\partial t} + \underbrace{\frac{\partial[\rho_s (1-\phi) v_s]}{\partial x}}_{Self-diffusion} = \dot{\xi}_s^{REV}. \tag{9b}$$

On the left hand side of Eq. 9a and Eq. 9b, the first terms are time derivatives and the second terms denote the self-diffusion terms via the gradient of fluid/solid velocity. The right hand side of Eq. 9 denotes the source/sink terms (i.e. the reaction part of the system). The thermodynamic fluxes that are triggered by cross-constituent diffusion are illustrated in Fig. 1. These source/sink terms stem from the possibility of cross-diffusion at a local scale.

Here we specify that $\dot{\xi}_f^{REV}$ denotes the REV-scale (Fig. 1a) averaging of mass transfer rate from the solid to the fluid phase, which equals to the mass loss rate of the solid skeleton. Likewise, $\dot{\xi}_s^{REV}$ is equivalent to the REV-scale averaging of mass loss rate in the fluid phase. Hence, the upscaling law is summarized as

$$\dot{\xi}_f^{REV} = -\frac{1}{V_{REV}} \int_{V_{REV}} \dot{\xi}_s^{local}, \tag{10a}$$

$$\dot{\xi}_s^{REV} = -\frac{1}{V_{REV}} \int_{V_{REV}} \dot{\xi}_f^{local}, \tag{10b}$$

where $\dot{\xi}_s^{local}$ and $\dot{\xi}_f^{local}$ denote the mass exchange rate in solid and in fluid phase at the local scale (Fig. 1b), respectively, which are affected by the local scale changes in porosity/permeability. Now we derive the mathematical expression for $\dot{\xi}_s^{local}$ and $\dot{\xi}_f^{local}$. Following the same procedure from Eq. 7 to Eq. 9, we can arrive at a local scale equivalent of the conservation equations:

$$\dot{\xi}_s^{local} = \frac{\partial[\rho_s(1-\phi^{local})]}{\partial t} + \underbrace{\frac{\partial[\rho_s(1-\phi^{local})v_s]}{\partial x}}_{Cross-diffusion}, \tag{11a}$$

$$\dot{\xi}_f^{local} = \frac{\partial[\rho_f\phi^{local}]}{\partial t} + \underbrace{\frac{\partial[\rho_f\phi^{local}v_f]}{\partial x}}_{Cross-diffusion}, \tag{11b}$$

where ϕ^{local} denotes the local scale porosity (see Fig. 1b).

This analysis shows that the reaction term requests a cross-diffusion term for closure. Both source and diffusion terms are coupled and cannot be chosen independently. Without considering this term explicitly and considering the interdependence of source and diffusion terms the equations become mathematically ill-posed as will be discussed later. It is furthermore important to note that at local scale the condition $\dot{\xi}_f^{local} + \dot{\xi}_s^{local} \neq 0$ can apply and thereby locally violate the overall entropy production. However, at wave sampling REV-scale the condition $\dot{\xi}_f^{REV} + \dot{\xi}_s^{REV} = 0$ holds. This directly leads to the definition of the cross-diffusion terms which spells out the local scale importance of the gradient terms of fluid/solid velocity in Eq. 11.

We emphasise the importance at identifying the local scale physics for the derivation of the cross-diffusion quantities as this is different to the *effective* formulation of diffusivity where the fast local scale diffusion processes are adiabatically eliminated (Biktashev and Tsyganov, 2016). The current approach requires looking at the actual diffusivities obtained by averaging the underlying physical processes rather than the effective lumped diffusivities of the conventional approaches. In other words, in our derivation of the REV sampled by the wave, the upscaled formulation still carries the information of the local scale processes instead of loosing it via lumping. We are now translating the information from density distribution to pressure distribution.

Through the homo-entropic flow assumption, ρ_f and ρ_s corresponds by the *Equation of state* to p_f and $\bar{p}_s$, respectively. Thereafter, Eq. 9a and Eq. 9b are respectively translated into Eq. 6a and Eq. 6b. In the context of pressure diffusion described by Eq. 6, we emphasise again that we explicitly separate the cross-diffusion terms from the source/sink terms considering the local scale processes and pass the information from local scale to REV-scale to combine with the self-diffusion part. Hence, a new actual diffusion

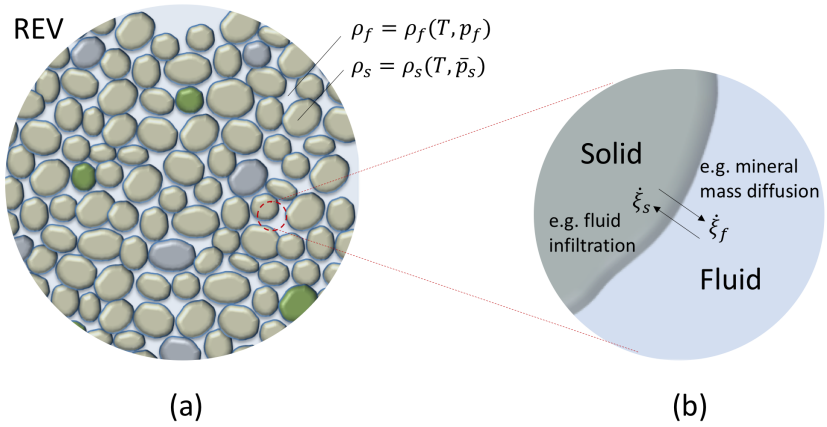

Figure 1: Sketch of a fully saturated porous medium: a) a REV sampled by a potential wave travelling through the medium, the density of each constituent is defined by equations of state: $\rho_f = \rho_f(T, p_f), \rho_s = \rho_f(T, \bar{p}_s)$; b) at pore-scale, where inter-constituent mass transfer occurs giving rise to possible wave instability. $\dot{\xi}_f$ denotes the rate of mass diffusing into the fluid phase from solid matrix (by e.g. mineral melting, mineral mass dissolution, grain crushing, internal erosion, clay dehydration), $\dot{\xi}_s$ the rate of fluid mass into the solid phase (by e.g. mineral precipitation, cementation, crystalization, fluid infiltration).

matrix is formed, with self-diffusion coefficients D_H, D_M (Eq. 6) being the diagonal elements (determined by the REV-scale porosity/permeability) and cross-diffusion coefficients h_1, h_2 the off-diagonal elements (determined by the local scale porosity/permeability).

5. Standing wave solution without cross-diffusion

We first consider Eq. 6 without cross-diffusion and consider simplifications to result in an equation with only two diffusion coefficients. In analogy to the Turing instabilities in chemical systems (Vanag and Epstein, 2009) we expect stable solutions or standing waves instabilities but no travelling waves. The first simplification is to assume an incompressible fluid. The next simplification is to assume quasistatic equilibrium. This is achieved by using the hypothesis of small perturbations with infinitesimal volumetric strain, in which case the Lagrangian and Eulerian approaches coincide to a first order approximation (Coussy, 2004). The small perturbation assumption is a strong simplification as it assumes that all time dependent material parameters vanish, i.e. the permeability must be constant on instability. This

implies that we assume that everywhere in the system the mechanical thermodynamic force is in equilibrium with the fluid thermodynamic force and consequently no time-dependent processes are triggered by their gradients.

5.1. Linear momentum balance

By neglecting the gravity component, linear momentum balance of a saturated body implies that the gradient of the effective stress is in static equilibrium with the gradient of the fluid pressure

$$\frac{\partial p'}{\partial x} = \frac{\partial p_f}{\partial x}. \tag{12}$$

Under these conditions the fluid pressure evolution collapses to a simple Darcy equation without Lagrangian reactive chemical source term and we obtain:

$$\frac{Dp_f}{Dt} = D_H \frac{\partial^2 p_f}{\partial x^2} + r^f, \tag{13a}$$

$$r^f = 0 \Rightarrow \frac{\partial p_f}{\partial t} = D_H \frac{\partial^2 p_f}{\partial x^2}. \tag{13b}$$

Likewise, for the standing wave assumption we assume that the wave velocity is zero and obtain the static mechanical viscoplastic overpressure diffusion equation:

$$\frac{Dx}{Dt} F_M = \lambda D_H \frac{\partial^2 \bar{p}_s}{\partial x^2} + r^M, \tag{14a}$$

$$\frac{Dx}{Dt} = 0 \Rightarrow \lambda D_H \frac{\partial^2 \bar{p}_s}{\partial x^2} = -r^M. \tag{14b}$$

Where λ is a non-dimensional parameter providing the link between the mechanics and fluid diffusion laws. The link can be derived from mass balance using mixture theory of the fluid-solid mixture.

5.2. Mass conservation without internal mass transfer

Without considering any internal mass transfer, Eq. 9 reduces to

$$\frac{\partial[\phi(v_f - v_s)]}{\partial x} + \frac{\partial v_s}{\partial x} = 0. \tag{15}$$

Using the simplification of constant permeability (Regenauer-Lieb et al., 2013) we have adopted Darcy's law for the fluid diffusion (Eq. 13b) which now applies to the fluid filter velocity is $\phi(v_f - v_s)$,

$$\phi(v_f - v_s) = -\frac{\kappa}{\mu_f}\frac{\partial p_f}{\partial x}. \tag{16}$$

Using following identities $\frac{\partial v_s}{\partial x} = \dot{\epsilon}_x = \dot{\epsilon}_v$ (Vardoulakis and Sulem, 1995; Coussy, 2004) the mass conservation equation can be written as,

$$\frac{\kappa}{\mu_f}\frac{\partial^2 \bar{p}_s}{\partial x^2} = \dot{\epsilon}_v, \; D_H \frac{\partial^2 \bar{p}_s}{\partial x^2} = \dot{\epsilon}_v. \tag{17}$$

Recall that $\bar{p}_s = \langle p' - p_y \rangle$ is the visco-plastic overpressure of the mixture above the yield stress p_y, $\dot{\epsilon}_v$ is the visco-plastic volumetric strain rate, μ_f the viscosity of the fluid and κ the permeability. The volumetric strain rate provides the link between solid and fluid diffusion. It is equivalent to the source term in Eq. 14b and $r^M = -\lambda\dot{\epsilon}_v$. Note that the mechanical and fluid diffusivities have unusual units $[\frac{m^2}{Pas}]$ as they include the unit stress in the denominator.

5.3. Cnoidal standing waves

For a linear source term the two diffusion equations do not feature instabilities. If, however, a non-linear mechanical source is chosen instabilities can occur. The key assumption for instabilities has been shown (Veveakis and Regenauer-Lieb, 2015; Regenauer-Lieb et al., 2013) to be a power law visco-plastic source term for $\dot{\epsilon}_v$ defined by:

$$\dot{\epsilon}_v = \dot{\epsilon}_{ref} \left\langle \frac{\bar{p}_s}{p'_{ref}} \right\rangle^m, \tag{18}$$

where p'_{ref} is a reference pressure for normalization. $\dot{\epsilon}_{ref}$ is here defined by the strain rate of the master process of far field compaction. The Macaulay bracket $\langle\cdot\rangle$ defines zero stress before yield p_y .

The resulting coupled solid-fluid poroviscoplastic reaction-diffusion equation therefore can be described by:

$$\frac{\kappa}{\mu_f}\frac{\partial^2 \bar{p}_s}{\partial x^2} = \dot{\epsilon}_{ref}\left\langle \frac{\bar{p}_s}{p'_{ref}} \right\rangle^m . \tag{19}$$

Introducing the following renormalizations:

$$\sigma^* = \frac{\bar{p}_s}{p'_{ref}}\ ,\ x^* = \frac{x}{L}, \tag{20}$$

where L is a reference length defined by the domain where boundary conditions are applied we can now identify the key dimensionless parameter for appearance of standing wave solutions as the ratio between the two diffusivities:

$$\lambda = \frac{D_M}{D_H} = \left(\frac{L}{\delta_c}\right)^2, \tag{21}$$

where δ_c is known as the compaction length (McKenzie, 1985). The mechanical diffusivity is D_M,

$$D_M = \frac{\dot{\epsilon}_{ref}\, L^2}{p'_{ref}}, \tag{22}$$

where $\dot{\epsilon}_{ref}$ is the strain rate used to define p'_{ref}. This is here chosen to be the background loading strain rate.

With these renormalizations the dimensionless form of Eq. 19 reduces to the long-wavelength solitary wave limit of the Korteweg de Vries equation (Veveakis and Regenauer-Lieb, 2015) :

$$\frac{\partial^2 \sigma^*}{\partial x^{*2}} - \lambda(\sigma^*)^m = 0, \tag{23}$$

λ describes the ratio of the mechanical diffusivity over the fluid diffusivity, i.e. the loading rate (strain rate $\dot{\epsilon}_{ref}$) over the diffusion rate of the pore fluid within the specimen of length L when subjected to load p'_{ref} on the boundary. It becomes intuitively obvious that if the mechanical load is faster by a critical factor (~ 10) than the ability of the fluid to escape then the solution to this equation must be an instability. In the above equation the instabilities appear as pressure wave-singularities in the form of sharp crests. A wave instability appears for any frequency higher than the lowest critical

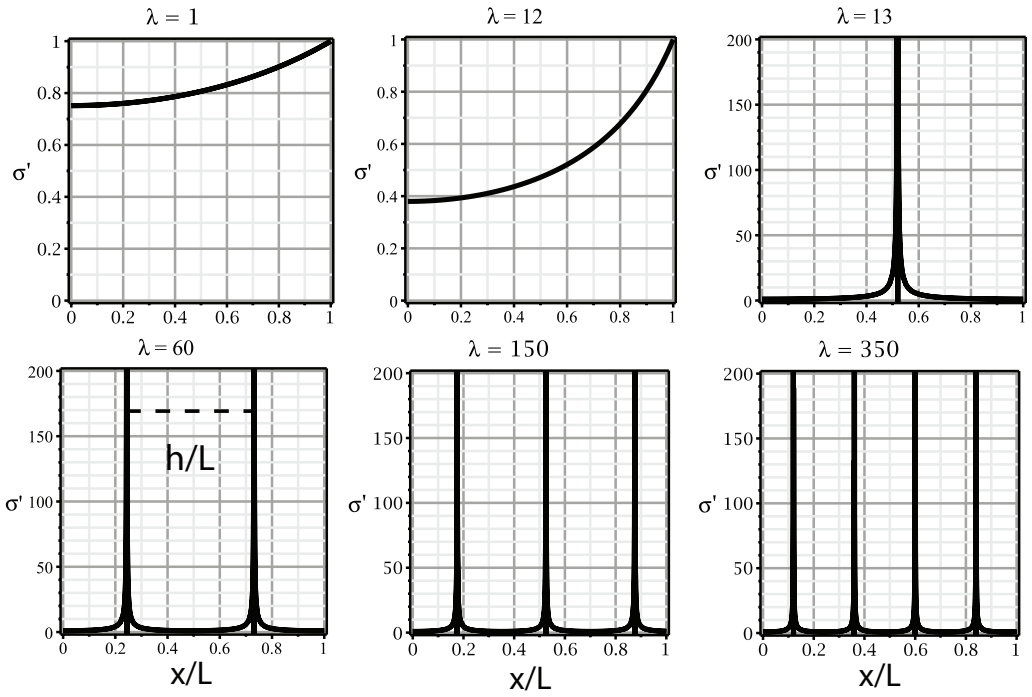

Figure 2: Cnoidal waves are periodic waves featuring overpressure of the weak phase. They are typically observed in the ocean as Tsunami events which are described by the Korteweg deVries equation of shallow water theory. The equation is sign invariant and can appear as a fluid channelling instability in rocks for compaction or dilation. Compaction and dilation waves can superpose linearly and form rectangular patterns parallel to the minimum and maximum principal stress, respectively.

Figure 3: Two generations of decimetre scale compaction bands (backpack for scale) in silt- and sandstones of the Miocene Whakataki formation, S of Castlepoint, North Island, New Zealand. The porosity reduction renders the bands less susceptible to erosion causing a marked positive relief. Cross-cutting generation of bands from top right to bottom left postdate earlier more regularly spaced bands and are interpreted as shear-enhanced compaction bands. The photo was supplied courtesy of Christoph Schrank.

frequency identified by a critical λ_{crit}. Any further loading above the critical limit creates more and more instabilities (higher frequency cnoidal waves). An example is shown in Fig. 2.

Note that the solution can apply to positive and negative σ^*, hence the standing waves are compaction or dilation bands. The distance between the dilatational or compactive overpressure channels is related to the compaction length δ_c, considering that the ratio of the pressure applied on the boundary over the corresponding strain rate corresponds to the secant viscosity of the solid matrix $\eta_s = \frac{p'_{ref}}{\dot{\epsilon}_{ref}}$ with the spacing h/L defined in Fig. 2,

$$\frac{h}{L} \approx \frac{4}{L}\delta_c = \frac{4}{L}\sqrt{\frac{\kappa\eta_s}{\eta_f}}, \tag{24}$$

5.4. Examples of standing cnoidal waves

The above described standing cnoidal wave equation has been proposed as a potential solution to a wide variety of geological phenomena that either contradict current understanding or are difficult to explain with current theories. These can be periodic channel network formations with a characteristic spacing of h as defined in Eq. 24. In nature the 1-D acceleration pressure wave approach must be combined with the acceleration shear waves (Veveakis and Regenauer-Lieb, 2015) leading to more complicated or transient wave patterns. A geological example of two sets of compaction bands, pure-compaction and shear-enhanced compaction bands, is shown in Fig. 3. Fig. 4 shows a close up view of the microstructure of a compaction band portraying a densification around the centre of the band. While the standing cnoidal wave approach does not provide information on the width of the compaction band it is clear from the figure that a diffusive gradient of grain crushing defines a finite width identified by the white dashed lines in Fig. 4. We will come back to this point in the following section when discussing the melt bands presented in Fig. 5.

Other examples from the literature include geological observations such as overpressurized impermeable shale (Alevizos et al., 2017); zebra striped banding in Mississippi Valley Type deposits (Kelka et al., 2017); periodic melt bands at right angles to the maximum principal stress in a partially molten gneiss (Weinberg et al., 2015; Veveakis et al., 2015) and in the laboratory a series of compaction bands in Tuffeau de Maastricht calcarenite, regularly spaced logarithmic spirals in borehole damage zones (Hu et al., 2017; Hu and Regenauer-Lieb, 2018) and Lüders bands due to martensitic transformations in mild steel, etc.(Veveakis and Regenauer-Lieb, 2015)

6. Waves with cross-diffusion

Before introducing cross-diffusion we discuss the classical scenario of two independent time scale processes for fluid and solid diffusion. The well-known Terzaghi consolidation theory of poro-elasticity considers a simplification that the process is entirely controlled by the timing of fluid diffusion. If the matrix is visco-plastic instead of purely elastic, a clay matrix for instance, the consolidation contains two time-dependent processes at different time-scales. The faster process is the diffusion of pore fluid which causes primary consolidation, while a secondary consolidation process is induced by the viscous micro-sliding of platelets that form the solid matrix of clay.

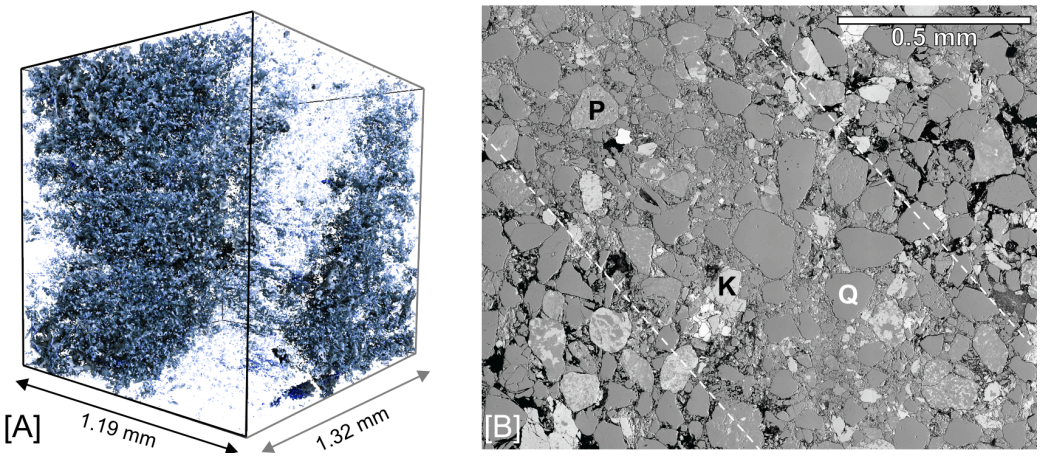

Figure 4: [A] X-Ray microtomograph of the density distribution around a compaction band in a fine grained sandstone, pores are shown as dark areas, the light area in between the dark zones corresponds to the compaction band. The tomogram is supplied courtesy of Fusseis (U.Edinburgh), X. Xia (APS, Argonne NL), D. Warne and M. Barry (HPC, QUT). [B] Back-scattered scanning electron microscope image (magnification factor 600) of compaction band showing crushed grains and loss of porosity (dark area) in the centre. P=Plagioclase, K= K-Feldspar and Q=Quartz. Approximate band boundaries are marked with white dashed lines. Porosity reduction within the band is due to grain crushing and mechanical pore collapse. The porosity (black pixels) outside the band shows the background porosity. Image courtesy of C. Ballington, S. Frischkorn, CARF (QUT).

Figure 5: Melt extraction channels in a partially molten metamorphic rock (gneiss) from the Sikkim Higher Himalaya Migmatite gneisses with two parallel vertical melt bands (leucosomes) forming in the hinges of two cuspate folds. The fold has been formed as a consequence of horizontal shortening implying that the direction of the maximum principal stress is also in the horizontal plane. The melt bands are perpendicular to the direction of the maximum principal stress and have been interpreted as standing cnoidal wave instabilities (Veveakis et al., 2015; Weinberg et al., 2015). We encounter three diffusional length scales that underpin the instability. The cnoidal wave length scale h which is controlled by the ratio of solid and fluid diffusivity λ, the melt extraction length scale l_1 which is related to the cross-diffusion coefficient h_1 and the thickness of the melt extraction channel l_2 which is related to the cross-diffusion coefficient h_2. Photo courtesy of Roberto Weinberg.

These micro-creep processes do not generally contribute to the fluid flow and the creep response is often well separated in time.

This allows the simplifying assumption of time-scale separation of primary (fluid controlled) consolidation and secondary (creep controlled) consolidation (Coussy, 2004). The uncoupled treatment of both processes can lead to standing wave instabilities, which normally only occur for cases of extremely slow fluid diffusion (low permeability) such as in the cases of a tight shale rock. This is characterised by Eq. 23 which defines a minimum critical λ_{crit} for instability. Prior to the stationary instability the cross-diffusional gradients are not likely to play a role for a perfectly homogeneous medium due to the stress continuity condition through the matrix.

However, upon the emergence of instabilities, the situation changes. The compacting layers are likely to introduce strong local gradients in fluid and overstress pressure around each compacting layer associated with local permeability changes, which introduces new time dependence and an interdependence of fluid and solid diffusion processes around the instability. The two time-step consolidation process can feed back on the new gradient terms and new wave dynamics can be expected for critical cross-diffusion parameters identified by Eq. 29.

6.1. Onset of Hydro-Poro-Mechanical wave instability

The new gradient terms can trigger wave instabilities as shown in the following linear stability analysis. In order to illustrate the important role of cross-diffusion in Eq. 6, we first neglect other possible source terms represented by r^F and r^M, and discuss linear stability only with the self-diffusion and cross-diffusion terms:

$$\begin{bmatrix} \frac{\partial p_f}{\partial t} \\ \\ \frac{\partial \bar{p}_s}{\partial t} \end{bmatrix} = \begin{bmatrix} D_H & h_1 \\ h_2 & D_M \end{bmatrix} \begin{bmatrix} \frac{\partial^2 p_f}{\partial x^2} \\ \\ \frac{\partial^2 \bar{p}_s}{\partial x^2} \end{bmatrix} \tag{25}$$

We apply a small plane wave perturbation to the system in the form of

$$\begin{bmatrix} p_f \\ \bar{p}_s \end{bmatrix} = \begin{bmatrix} p_f \exp\left(ikx + st\right) \\ \bar{p}_s \exp\left(ikx + st\right) \end{bmatrix} \tag{26}$$

where k and s denote the variable wavenumber (in space) and frequency of the perturbation, respectively. The assumption of small perturbation is a classical one in solid mechanics, however, it is worthwhile to briefly discuss

its role in the context of the fluid-like motions of the solid matrix and the fluid seepage through the pore space as discussed in this paper.

In this context the small perturbation provides necessary conditions for fluid diffusion and advection driven instabilities as a local spatial departure from the background steady state. These small wavelength instabilities are in turn driven by the large scale applied gradients thus providing the condition for initiation of spatio-temporal patterns, i.e. travelling waves, for critical parameters. They manifest themselves as local advection of the pore fluid making room for the matrix to compact and propagate in an accordion-like motion to leave permanent small amplitude compaction in its wake.

Substituting Eq. 26 into Eq. 25, we can then derive a characteristic equation of s:

$$s^2 + (D_H k^2 + D_M k^2)s + (D_H D_M - h_1 h_2)k^4 = 0 \tag{27}$$

Then the determinant of Eq. 27 is obtained:

$$\Delta = (D_H k^2 + D_M k^2)^2 - 4(D_H D_M - h_1 h_2)k^4 \tag{28a}$$

$$= k^4[(D_H - D_M)^2 + 4h_1 h_2] \tag{28b}$$

The condition for instability to appear is $\Delta < 0$ for all k, which hence requires

$$(D_H - D_M)^2 + 4h_1 h_2 < 0 \tag{29}$$

Eq. 29 indicates that a necessary condition for Hydro-Poro-Mechanical wave instability (neglecting r^f and r^M in Eq. 6) to occur is that the cross-diffusion coefficients h_1 and h_2 are non-zero and of opposite sign. For the scenarios without cross-diffusion, the eigenvalues of characteristic Eq. 27 only consist of real parts (i.e. $\Delta \geq 0$) and hence no wave instability exists.

Now we further discuss the role of a possible source term. Following the results in Section 5 and considering a source term r^M in the form of $-\lambda \bar{p}_s^m$ as shown in the Cnoidal equation (see Eq. 23), the characteristic equation of the coupled system becomes

$$(s + k^2 D_H)(s + k^2 D_M + \lambda exp[(ikx + st)(m-1)]) - h_1 h_2 k^4 = 0 \tag{30}$$

If we consider a simple case of $m = 1$, the determinant of Eq. 30 turns to be

$$\Delta = (k^2 D_H - k^2 D_M - \lambda)^2 + 4h_1 h_2 k^4. \tag{31}$$

Then the emergence of instability under $\Delta < 0$ requires

$$(D_H - D_M - \frac{\lambda}{k^2})^2 + 4h_1 h_2 < 0, \tag{32}$$

where the wavenumber of the perturbation k now plays a role. For a large enough wavenumber, $\frac{\lambda}{k^2}$ vanishes and Eq. 32 reduces to Eq. 29. On the other hand, when looking at smaller wavenumbers Eq. 32 shows that a critical wavenumber exists below which instabilities are no longer possible. It is worth mentioning that for a general wave instability described by Eq. 32, it remains a necessary condition for the cross-diffusion coefficients h_1 and h_2 to be non-zero and of opposite sign.

6.2. Field example of cross-diffusion instability

The length scales defined by the diffusion gradients provide additional information on *in situ* material properties. We noted in Fig. 4 that there is a gradient of grain crushing causes a densification towards the centre of the compaction band. This gradient may be interpreted as evidence of cross diffusion. In order to further illustrate possible cross-diffusion gradients, we discuss a melt extraction example Fig. 5 where slower process of complex interplay between melt viscosity and matrix viscosity reveal additional length scales.

In order to understand the geological process leading to transient cross-diffusion fronts it is, however, useful to first discuss the rock formation prior to the lateral compression causing the instability. A migmatite is a mixture of metamorphic rock (here Sikkim Higher Himalaya gneisses) and partial melt or crystallized partial melt (here gneissic partial melts). This leads typically to the separation of minerals assemblages with lighter and darker layers with a layered pattern. The lighter melt products are leucosomes which consist of granitic mineralogy with a lower melting point, while the darker layers are amphibole and biotite rich. The partially molten rock is modelled as a porous two-phase medium with the melt playing the role of viscous fluid and the solid matrix assumed to be viscoplastic.

Fig. 5 shows the melt channels explained by (Weinberg et al., 2015; Veveakis et al., 2015) as the filter pressing of melt out of solid matrix for a critical λ_{crit}. Under the standing cnoidal wave assumption the distance h between instabilities can be used to invert for diffusive material properties as it is a function of the viscosity of the melt, the viscosity of the matrix and the permeability. However, on closer inspection of Fig. 5 three characteristic length scales can be identified.

Though the transient aspects of the geological process are difficult to assess and a simpler interpretation as a standing wave (Weinberg et al., 2015) may be preferred, we interpret these length scales as evidence for incipient

transient cross-diffusional waves. The transient nature of the process can be inferred from Fig. 5 as the melt extraction process in the vertical channels (lightly coloured material) apparently has stopped before extracting all available melts (now crystallized). A considerable amount of melt appears to be still trapped between the vertical extraction channels.

In order to explain these length scales in terms of diffusional wave fronts of Eq. 6 we consider a a symmetry condition as the basis of our coordinate system. This symmetry condition is placed at the origin of the future melt band instability and can be viewed as an impermeable surface. Upon inception of instability, compaction of the viscoplastic matrix starts making room for melt flow through the porous matrix towards the origin of the coordinate system. The onset of the instability is a step function in time and the diffusive flow of melt towards the origin is characterised by the error function solution to the diffusion flow, while the compaction of the matrix is described by the complementary error function with an opposite flux direction. If we now consider the origin to be in a Lagrangian reference frame moving with the wave velocity $\frac{Dx}{Dt}$ we can identify three diffusive length scales associated with the instability.

The first diffusion length scale is the distance between the melt extraction bands h which is defined by the ratio of $\frac{D_M}{D_H}$ resulting in Eq. 21. The characteristic time τ is defined by the diffusion time of the macroscale instability. Following Coussy (2004) this time scale is the time scale for the slower process, i.e. secondary consolidation, which is controlled by the background strain rate of the deformation process in Eq. 18 and hence $\tau = \frac{1}{\dot{\epsilon}_{ref}}$. The second diffusion length scale l_1 describes the diffusion front of Darcy flow of melt into the melt band for the finite time scale of fluid flow into the melt band instability. If we define the diffusion length as a decay of fluid pressure by 0.84 times its maximum value then the width is $l_1 = 2\sqrt{|h_1|\tau}$. The third diffusion length scale is the thickness of the melt band itself l_2 which is characterized by the rapid decay of the volumetric strain rate $\dot{\epsilon}_v$ over the time of the instability close to the melt band. This length scale is defined by the diffusion length of the overstress $\bar{p_s}$ via the power law relation in Eq. 18, hence it is characterized by an opposite direction of diffusion with $l_2 = 4\sqrt{|h_2|\tau}$ due to symmetry.

The length scales h and l_2 are clearly visible in the photograph. The diffusion length l_1 is identified as the region close to the melt extraction channels, where the dark and light layers are more tightly packed. The transition re-

gion from densely spaced bands to wider bands is here interpreted to mark the distance of the diffusive melt extraction region (the transition point is near the tip of the finger in Fig. 5. The interpretation is based on the observation that the central area between the two melt channels shows relatively thick leucosomes suggesting that the melt extraction instability did not have sufficient time to reach the central area. Cross-diffusion in this outcrop refers to the diffusion pressure in the bulk matrix due to the mechanical filter pressing of the lightly coloured melts into the vertical melt extraction channels. Accordingly, the mechanical instability in the melt channel is interpreted to have generated a transient local gradient in matrix pressure that causes a diffusion flux around the melt channel while the fluid flux in turn leads to a local relaxation of the mechanical overpressure.

6.3. Laboratory example of cross-diffusion

We now consider the more general case where multiple diffusional processes are coupled. As expected from the earlier discussion this situation can lead to the additional cross-diffusion waves with a rich solution space. The simplicity of the approach is not lost even under consideration of higher order terms.

For a system consisting of n-constituents, Eq. 6 can be generalized as

$$\begin{bmatrix} \frac{\partial p_1}{\partial t} \\ \vdots \\ \frac{\partial p_n}{\partial t} \end{bmatrix} = \begin{bmatrix} D_{11} & D_{12} & \dots \\ \vdots & \ddots & \\ D_{n1} & & D_{nn} \end{bmatrix} \begin{bmatrix} \frac{\partial^2 p_1}{\partial x^2} \\ \vdots \\ \frac{\partial^2 p_n}{\partial x^2} \end{bmatrix} + \begin{bmatrix} r_1 \\ \vdots \\ r_n \end{bmatrix}. \tag{33}$$

Similarly, applying a small perturbation to Eq. 33, the determinant of the resulting characterization equation defines the criterion for transient cross-diffusional wave instabilities to nucleate.

We discuss two examples of the generalization of the approach with three components: solid matrix, fluid and crushed grains. The first example is shown in Fig. 6a where an oedometric compression experiment is performed on a brittle porous medium (puffed rice packs). The drainage condition for the consolidation process is the top of the container. Instabilities are observed to nucleate at the bottom of the porous medium and solitary compaction waves are observed to propagate upwards at a speed an order of magnitude faster than the loading rate. When the wave hits the top of the sample an acoustic emission is detected and a new wave nucleates at the bottom of the

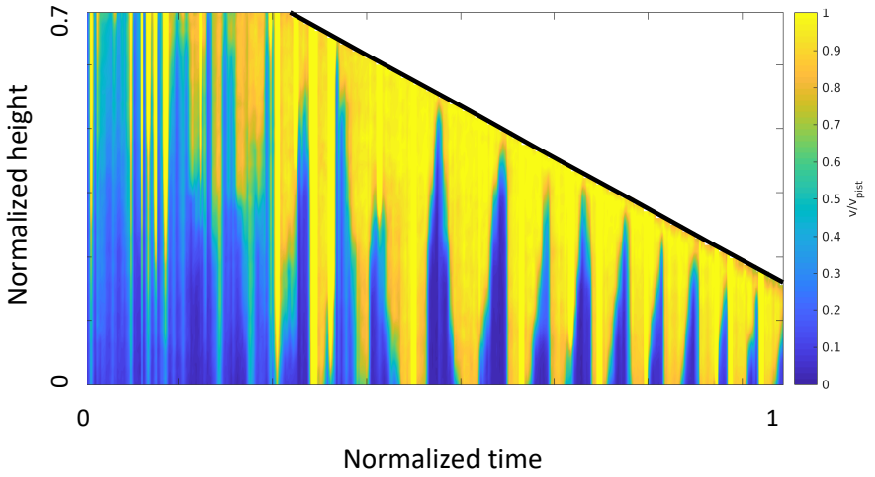

(a)

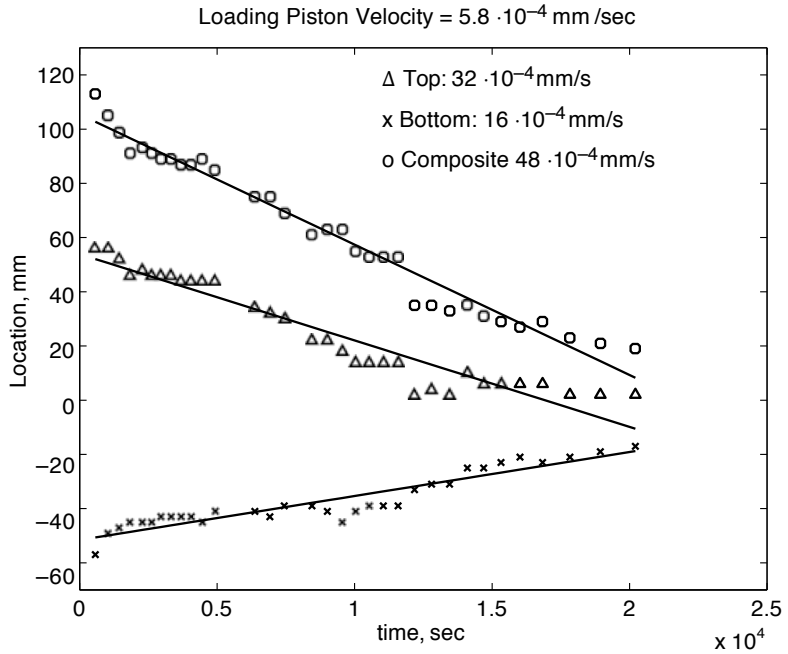

(b)

Figure 6: Travelling wave observed in oedometric compression tests as propagating compaction bands: a) in a brittle porous granular medium (Guillard et al., 2015) with contours of recorded local velocity, photo courtesy of James Baker; b) in Castlegate Sandstone (Olsson, 2001) with traces of compaction fronts identified by acoustic emission.

sample. The process continues until the sample is compacted to around 20% of the original height.

Cross-diffusion can be used to interpret these observations considering three phases in the system: the escaping air, the coarse solid skeleton and the crushed powdered grains. Consequently, the solid consolidation occurs through two independent mechanical processes. One is the granular media flow of the solid matrix leading to a denser packing of the grains upon compaction, the other is a phase transition of the grains into a powder. The interaction between the compaction of the solid matrix and the escaping air is not likely to cause cross-diffusion because the time scales of the two diffusion process are far apart. The air readily escapes compared to the frictional rearrangement of grains under compaction. However, upon crushing of the grains the generation of mass in the powder phase introduces a new time-scale process that links the diffusion of the escaping air with the compaction (/crushing as internal erosion) of the solid matrix, which corresponds to the cross-diffusion terms in Eq. 6. Two mass/pressure diffusion fluxes of opposite direction are introduced, leading to the cross-diffusion coefficient h_1 and h_2 having opposite sign. If the product of h_1 and h_2 becomes large enough to fulfil Criterion 29 cross-diffusion waves nucleate.

We may expect fluid-mechanical instabilities in a (fluid-like) granular medium, however, whether the approach also holds for porous rocks is still an open question. Here we refer to an experiment performed with a porous sandstone (Castlegate Sandstone) where a singular propagating wave has been identified without multiple nucleations (see Fig. 6b). The key observation of a travelling compaction wave speed an order of magnitude larger than the loading velocity is reproduced, however, in this case the wave instability propagates from both ends (with the drainage condition at the top and the bottom) and meets approximately in the median line.

7. Discussion

The mathematical simplification of a rigid-viscoplastic porous medium (Hill, 1954) allows merging insights from fluid mechanics with those from classical plasticity theory. Hill (1954) points out the analogy between the characteristics in supersonic flow of a fluid (Mach Lines) with the characteristics in the hyperbolic region of a plastic solid (Slip Lines). Accordingly, subsonic flow corresponds to the elliptic part of a plastic zone. Hill (1954) also notes that there is a striking contrast between the respective available

methods, which are more adaptive in fluid flow. He defers the question whether these can be taken over and applied in the plastic field to a matter for further study.

In this paper we have picked up these threads and investigated wave phenomena that are related to the Korteweg-de Vries equation discussed here in its solitary long-wavelength limit (Eq. 23). This equation is famous for its application as a mathematical model of waves on shallow water surfaces resulting in the long wavelength limit into the propagation of solitons (Le Mehaute, 1976). Cross-diffusional waves discussed here are different to classical solitons.They have been classified as a new-type of wave phenomenon (Tsyganov et al., 2007) first encountered in Laser optics as quasi-solitons (Paschotta, 2008). They can appear in a similar singular form as a simple quasi-soliton wave or can have complex shapes as envelope quasi-solitons or multi-envelope quasi-solitons (Tsyganov and Biktashev, 2014).

The investigation of these waves is a promising avenue for future studies, requiring the design of new experimental methods for quantitative assessments. In this study potential field and laboratory applications have been discussed in a qualitative manner as the experiments have not been performed to test the working hypothesis of travelling wave solutions. These experiments are part of ongoing work requiring relaxation of the mathematical idealisation of rigid-viscoplastic porous media and the assumption of homo-entropic flow.

For laboratory verification we shall further consider the effect of internal mass transfer with elasticity, the effect of elastic stress-diffusion with temperature-dependent material coefficients, the effect of internal chemical processes, etc. For the fluid analogy to hold we also need to specify the effect of finite strain. We have already pointed out that the addition of thermal gradients implies a natural extension of the diffusion matrix by the temperature reaction-diffusion equation. Thermodynamic consistency is satisfied for waves with thermomechanical coupling which can oscillate between adiabatic and isothermal limits leading to a flutter like phenomenon (Benallal and Bigoni, 2004). For thermodynamic consistency of incompressible (Malek and Rajagopal, 2006), compressible (Heida and Malek, 2010) and finite strain (Malek et al., 2018) Korteweg-type fluids we refer to the fluid dynamics literature. Here, we briefly discuss an extension from the perspective of Airy stress potential to include the effect of elasticity and its interplay with internal mass transfer. Interestingly, this phenomenologically based extension finds itself converged to the presented cross-diffusion framework.

7.1. Internal mass transfer at local scale satisfying compatibility

The effect of mass transfer rate on the constitutive relation of a degrading elasto-plastic material subject to mineral dissolution is discussed in (Hu and Hueckel, 2013, 2019). In the plastic domain (Hu and Hueckel, 2013), the yield surface is affected by the mechanical stress invariants, the deviatoric strain hardening, as well as a time integration of mineral mass transfer. The internal mass transfer rate is linked to newly generated crack surfaces by micro-cracking, i.e. the irreversible deformation/strain field, via the total specific surface area of the REV.

In this sense, internal mass transfer at local scale provides a constitutive link between stress (i.e. a generalized force) and strain rate (i.e. a generalized flux). For the quasi-elastic regime (Hu and Hueckel, 2019), the effective elastic modulus is coupled with the time integration of internal mass transfer, through a chemical shrinking mechanism in analogy to heat expansion in thermoelasticity (Nowacki, 1962). By satisfying compatibility equation, an additional term (induced by internal mass transfer) appears in the biharmonic Airy stress function, leading to a Poisson's equation for the particular solution of the extended Airy potential:

$$\nabla^2\Phi^{(p)} = -\frac{E\tilde{\alpha}}{1-\nu^2}\cdot\int_0^t \dot{\xi}d\tau. \tag{34}$$

where $\Phi^{(p)}$ denotes the particular (p) solution of the extended Airy potential. E denotes the initial elastic modulus and ν the Poisson ratio. $\tilde{\alpha}$ is the chemical deformation coefficient being affected by local specific surface area. $\dot{\xi}$ denotes the mass loss rate from the solid skeleton, which is equivalent to $\dot{\xi}_f$ in the current framework.

Note that $\nabla^2\Phi$ corresponds to the first invariant of the stress tensor, and hence can represent the volumetric mean effective stress. $\nabla^2\Phi^{(p)}$, as a (p) part of the solution, represents the effect on the volumetric mean effective stress introduced by internal mass transfer. Taking a time derivative of Eq. 34, we recover the source term in the (M) process, which by non-adiabatic relaxation gives rise to the cross-diffusion term in Eq. 6b.

7.2. Other diffusional wave phenomena

The similarity of the governing PDE's to other energetic fields where similar wave phenomena have been observed may allow us to transfer knowledge. The approach is in fact analogous to molecular-scale wave mechanics, which

has gained enormous success in computational chemistry. In this theory the time-independent stationary state limit of Schrödinger's diffusional wave equation yields electronic structures known as atomic orbitals. Linear superposition of atomic orbitals can be used to derive energy eigenstates of complex molecular orbitals for solid-state physics (Dronskowski and Hoffmann, 2008). At molecular-scale, the wave mechanics approach has also been extended to investigate dynamic interactions and stability limits at nano-scale such as during nano-indentation (Li et al., 2002) and solid-liquid interactions (Cheng et al., 2001).

Li et al. (2002) emphasizes that the yield phenomenon in crystals is based on acceleration waves nucleated at atomistic scale equivalent to the continuum-based condition for macroscopic shear localization phenomenon of Lüder bands in metals introduced by Hill (1962) and for shear localization in general solids by Rice (1976). From a molecular dynamics perspective, the yield phenomenon thus is a manifestation of satisfying the time-dependent localization criterion for the evolution of internal processes in a continuum.

Perhaps the most well studied field of cross-diffusion waves is in chemistry (Vanag and Epstein, 2009). If we replace the energetics of solid/fluid pressure by concentration of chemical species and the pressure diffusivities with chemical diffusivities of the different species in Eq. 6 (or more generally, Eq. 33) we obtain the equivalent cross-diffusion equations for a pure chemical system. Also, it is found that Turing instabilities can occur in systems with two independent diffusion coefficients (Vanag and Epstein, 2009), leading to patterns that are stationary in time but periodic in space.

Turing instabilities are steady state spatially inhomogeneous solutions which appear because linearly unstable eigenfunctions are growing exponentially with time. This leads in the cnoidal-wave case (a Turing pattern) discussed in Fig. 2 to infinite pressure on the singularities. The solution hence does not satisfy criteria for well-posedness. Vardoulakis (2001) discussed reaction-diffusion equations for fault modelling, which led to a similar ill-posed negative diffusion problem in time. The problem was stabilized via introduction of a non-linear source term playing the role of a positive cross-diffusion term in the mechanical conservation equation.

Such cross-diffusion systems, consisting of three or more independent dynamic coefficients in the underpinning cross-diffusion PDE's, can lead to wave instabilities. This type of transient instability, characterized by both spatial and temporal periodicities, has the potential for allowing complex wave interactions. Typically, the dynamic cross-diffusion coefficients need to

be significant enough to compete with the self-diffusion process giving rise to the nucleation of transient cross-diffusion waves.

8. Conclusions

We have introduced a new approach to Hydro-Poro-Mechanical coupled instabilities using the simple concept of cross-diffusion. Our work revealed a number of excitable wave phenomena in mechanics of solids that are akin to their elastic counterpart (Cartwright et al., 1997) but do not carry inertial effects and are entirely triggered by the coupling of the diffusion and cross-diffusion coefficients. We have shown field and laboratory examples, where only two self-diffusion coefficients interact constructively to cause a standing cnoidal wave instability. The criterion for instability and the wavenumber of the standing wave is characterised by the parameter λ, which is defined by the ratio of mechanical and fluid diffusivity. If cross-diffusion terms are added the propensity for instabilities is significantly enhanced and a rich class of propagating dissipative wave phenomena in the form of travelling waves is revealed.

The wave phenomena are predicted for a broad range of multiphysics pattern formation in Hydro-Poro-Mechanical materials. The approach allows a fundamental physics/chemistry-based view of the initiation of instabilities and the transient waves around the formation of stationary waves defining the material instabilities. Future extension of the approach will investigate the superposition of volumetric and shear wave instabilities, allowing the interpretation of features such as compaction bands, and fault patterns to be modelled under a new wave mechanics perspective. We are currently investigating these wave phenomena in controlled laboratory experiments and attempt to use the unique relationship of spectral content of the waves as well as observations of the amplitude and wave speed as a diagnostic tool for data assimilation of self- and cross-diffusional material properties.

9. Acknowledgments

This work was supported by the Australian Research Council (ARC DP170104550, DP170104557) and the strategic SPF01 fund of UNSW, Sydney.

References

Alevizos, S., Poulet, T., Sari, M., Lesueur, M., Regenauer-Lieb, K., Veveakis, M., 2017. A framework for fracture network formation in overpressurised impermeable shale: Deformability versus diagenesis. Rock Mechanics and Rock Engineering 50 (3), 689–703.

Atkinson, J., 2014. Fundamentals of Ground Engineering. Apple Academic Press Inc., Country Oakville, Canada.

Benallal, A., Bigoni, D., 2004. Effects of temperature and thermo-mechanical couplings on material instabilities and strain localization of inelastic materials. Journal of the Mechanics and Physics of Solids 52 (3), 725.

Biktashev, V. N., Tsyganov, M. A., 2016. Quasisolitons in self-diffusive excitable systems, or why asymmetric diffusivity obeys the second law. Scientific Reports 6, 30879.

Cartwright, J. H. E., Hernández-García, E., Piro, O., Jul 1997. Burridge-knopoff models as elastic excitable media. Phys. Rev. Lett. 79, 527–530.

Cheng, L., Fenter, P., Nagy, K. L., Schlegel, M. L., Sturchio, N. C., 2001. Molecular-scale density oscillations in water adjacent to a mica surface. Physical review letters 87 (15), 156103.

Coussy, O., 2004. Poromechanics. Wiley, Chichester.

Dronskowski, R., Hoffmann, R., 2008. Computational Chemistry of Solid State Materials: A Guide for Materials Scientists, Chemists, Physicists and others. Vol. VI. Wiley-VCCH, Weinheim.

Guillard, F., Golshan, P., Shen, L., Valdes, J. R., Einav, I., 2015. Dynamic patterns of compaction in brittle porous media. Nature Physics 11, 835–838.

Heida, M., Malek, J., 2010. On compressible korteweg fluid-like materials. International Journal of Engineering Science 48 (11), 1313–1324.

Hill, R., 1954. On inoue‘s hydrodynamic analogy for the state of stress in a plastic solid. Journal of Mechanics and Physics of Solids 2, 110–116.

Hill, R., 1962. Acceleration waves in solids. Journal of the Mechanics and Physics of Solids 10 (1), 1–16.

Hu, M., Hueckel, T., 2013. Environmentally enhanced crack propagation in a chemically degrading isotropic shale. Geotechnique 63 (4), 313–321.

Hu, M., Hueckel, T., 2019. Modeling of subcritical cracking in acidized carbonate rocks via coupled chemo-elasticity. Geomechanics for Energy and the Environment.
URL https://doi.org/10.1016/j.gete.2019.01.003

Hu, M., Regenauer-Lieb, K., 2018. Entropic limit analysis applied to radial cavity expansion problems. Frontiers in Materials 5, 47.

Hu, M., Veveakis, M., Poulet, T., Regenauer-Lieb, K., Nov 2017. The role of temperature in shear instability and bifurcation of internally pressurized deep boreholes. Rock Mechanics and Rock Engineering 50 (11), 3003–3017.

Kelka, U., Veveakis, M., Koehn, D., Beaudoin, N., 2017. Zebra rocks: compaction waves create ore deposits. Scientific Reports 7 (1), 14260.

Le Mehaute, B., 1976. An Introduction to Hydrodynamics and Water Waves. Springer-Verlag, New York.

Li, J., Van Vliet, K. J., Zhu, T., Yip, S., Suresh, S., 2002. Atomistic mechanisms governing elastic limit and incipient plasticity in crystals. Nature 418 (6895), 307–310.

Malek, J., Prusa, V., Skrivan, T., Suli, E., 2018. Thermodynamics of viscoelastic rate-type fluids with stress diffusion. Physics of Fluids 30 (2), 023101.

Malek, J., Rajagopal, K. R., 2006. On the modeling of inhomogeneous incompressible fluid-like bodies. Mechanics of Materials 38 (3), 233–242.

McKenzie, D., 1985. The extraction of magma from the crust and mantle. Earth and Planetary Science Letters 74, 81–91.

Nowacki, W., 1962. Thermoelasticity. Addison-Wesley, Reading, MA.

Olsson, W. A., 2001. Quasistatic propagation of compaction fronts in porous rock. Mechanics of Materials 33 (11), 659 – 668.

Paschotta, R., 2008. Quasi-Soliton pulses, 1st Edition. Wiley-VCH.

Perzyna, P., 1966. Fundamental problems in viscoplasticity. Adv. Appl. Mech. 9, 243–377.

Regenauer-Lieb, K., Veveakis, M., Poulet, T., Wellmann, F., Karrech, A., Liu, J., Hauser, J., Schrank, C., Gaede, O., Fusseis, F., 2013. Multiscale coupling and multiphysics approaches in earth sciences: Applications. Journal of Coupled Systems and Multiscale Dynamics 1 (3), 1–42.

Rice, J. R., 1976. The localization of plastic deformation. North-Holland, Amsterdam, pp. 207–220.

Rice, J. R., Cleary, M. P., 1976. Some basic stress diffusion solutions for fluid-saturated elastic porous media with compressible constituents. Reviews of Geophysics and Space Physics 14 (2), 227–241.

Rudnicki, J., Rice, J., 1975. Conditions for the localization of deformation in pressure sensitive dilatant materials. J. Mech. Phys. Solids 23, 371–394.

Tsyganov, Mikhail, A., Biktashev, V. N., Brindley, J., Holden, A. V., Genrikh, R. I., 2007. Waves in systems with cross-diffusion as a new class of nonlinear waves. Physics-Uspekhi 50 (3), 263.

Tsyganov, M. A., Biktashev, V. N., Dec 2014. Classification of wave regimes in excitable systems with linear cross diffusion. Phys. Rev. E 90, 062912.

Vanag, V. K., Epstein, I. R., 2009. Cross-diffusion and pattern formation in reaction–diffusion systems. Physical Chemistry Chemical Physics 11 (6), 897–912.

Vardoulakis, I., 2001. Thermo-poro-mechanics of rapid fault shearing. Springer Berlin Heidelberg, Berlin, Heidelberg, pp. 63–74.

Vardoulakis, I., Sulem, J., 1995. Bifurcation Analysis in Geomechanics. Blankie Acc. and Professional, Glasgow.

Veveakis, E., Regenauer-Lieb, K., 2015. Cnoidal waves in solids. Journal of the Mechanics and Physics of Solids 78, 231–248.

Veveakis, E., Regenauer-Lieb, K., Weinberg, R. F., 2015. Ductile compaction of partially molten rocks: The effect of non-linear viscous rheology on instability and segregation. Geophysical Journal International 200 (1), 519–523.

Weinberg, R., Veveakis, M., Regenauer-Lieb, K., 2015. Compaction bands and melt segregation from migmatites. Geology 43 (6), 471–474.